eV-TEM: transmission electron microscopy with few-eV electrons

Geelen, D.

Chapter 5

Spectroscopy II: Inelastic processes

Electrons moving through a material can transfer energy to this medium via many different processes, e.g. electron-phonon and electron-plasmon interaction among others. It is important to have a good understanding of such processes as they are responsible for radiation damage. For instance, they are of key importance in the study of biological materials with electron microscopy. In **E**xtreme **U**ltra**V**iolet (EUV) photolithography, the damage caused by LEE is significant (as we will see in the next chapter). Moreover, the spectra presented in chapter 4 are strongly influenced by loss processes. The unique capability of our improved Leiden ESCHER microscope, that allows both transmission and reflection measurements, enables us to study the electron energy losses as a function of position with a high spatial resolution. Additionally, we perform **E**lectron **E**nergy **L**oss **S**pectroscopy (EELS) measurements in the ESCHER microscope. We find several energy loss processes such as the π and $\pi + \sigma$-plasmon losses in graphene.

5.1 Inelastic scattering

Electrons entering a material interact with its constituents through a variety of interaction and excitation mechanisms. As a result, energy and momentum is transferred to the material, changing the direction and velocity of the incident electrons.

We distinguish two kinds of scattering: elastic and inelastic. In elastic scattering incident electrons mainly interact with the nuclei in the sample. Electrons in the material are involved since they screen the electric field of the nuclei. Usually only the direction of motion of an electron is changed. Atomic nuclei are thousands of times more massive than electrons, the energy transfer is therefore negligible* and we cannot detect it for the LEE in our instrument. Elastic electron scattering in a crystal leads to the formation of diffracted beams. Phonons, collective motions of the nuclei in a crystal, can also be excited due to scattering. The energy transfer involved in the excitation of phonons is in the order of ~ 0.1 eV [3, 4]. This is often referred to as quasi-elastic scattering.

In inelastic scattering, incident electrons interact with the electrons in the material. The energy transfer can therefore be much more significant than in elastic scattering. The energy transfer excites electrons in the material to previously unoccupied higher energy levels. In conductors, this can be an intraband transition to a state above the Fermi level. In insulators and semiconductors the transitions will primarily be interband transitions across the band gap. Some transitions set collective excitations of the valence electrons in motion. Such collective motions are called plasmons. When an electron from the material is excited to an energy level that lies above the vacuum level, it can escape the material. In this case the electron from the material is emitted as a secondary or Auger electron.

*This is only true for low-energy electrons. When a 100 keV (in conventional TEM) is backscattered over 180° (i.e. reflected) from carbon, the incident electron transfers an energy of ~ 18 eV to the sample. This is enough to displace carbon atoms from their lattice positions and leave the material (electron-beam sputtering) [1, 2].

(a) Mirror mode -2 eV

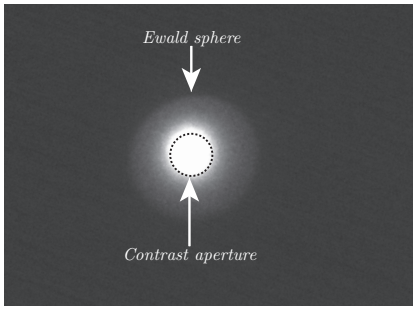

(b) LEEM diffraction 4.2 eV

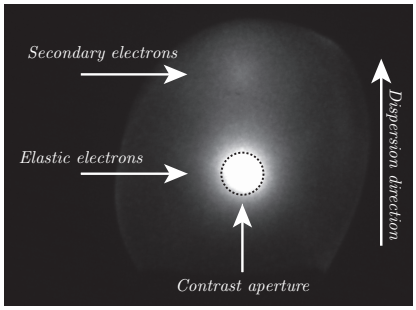

(c) LEEM diffraction 25 eV

Figure 5.1: (a) Reflection mirror mode in diffraction. Electrons are reflected back into the imaging system before they reach the sample. This is therefore the unperturbed signal. **(b)** The Ewald sphere of 4.2 eV reflected electrons. Most electrons end up close to the center of the sphere. **(c)** The Ewald sphere of 25 eV reflected electrons. Here the inelastically scattered electrons are visible in the top half of the diffraction plane.

In some cases the excitations of electrons to higher energy states induce changes in the material. An example is the H_2^+-ion. A transition of the electron in this configuration from the bonding to the antibonding state, will cause the ion to fall apart. This is a case of radiation or ionization damage. This mechanism of the disruption or breaking of molecular bonds is especially relevant in organic compounds.

As a consequence of the (loss) processes an electron underwent in the material, the outgoing electrons have a different momentum and energy distribution than the incoming electrons. The outgoing electrons therefore carry information about the interactions between LEE and the material.

5.2 Inelastic scattering in ESCHER

As explained in chapter 2, the energy and momentum distribution can be studied in the diffraction plane. Figure 5.1 shows the diffraction patterns of a freestanding graphene monolayer illuminated with different electron energies (these are reflected electrons). Figure 5.1a is measured in mirror-mode where all electrons are reflected back in the imaging system before they hit the sample. Provided the electric field does not have an out-of-plane component (when the electron energy is sufficiently negative or when the sample surface is sufficiently flat), the incident electron beam is therefore unperturbed.

In figure 5.1b the diffraction plane of reflected electrons is shown. The incident electrons hit a freestanding graphene monolayer with 4.2 eV. The specular spot is significantly broader than the unperturbed beam in mirror-mode. Locatelli et al. argue that this spot broadening is a consequence of corrugation of the surface [5].

Figure 5.1c shows the diffraction pattern in reflection that is formed when the graphene layer is illuminated with 25 eV electrons. The specular spot is very similar to the spot in figure 5.1b. Most elastically scattered electrons leave the surface close to the surface normal. However, a large blob can be seen in the top of the diffraction pattern. These are both electrons that have lost energy due to inelastic processes and secondary electrons. Since these electrons leave the sample with a lower energy than the specular electrons, they are deflected over a different angle by the MPA (see section 2.1.4) and thus end up at a different position in the diffraction plane.

As explained in section 2.1.4 the energy loss spectrum can be imaged by inserting a slit in the backfocal-plane of the objective lens.

5.3 Electron energy-loss spectroscopy

The unique capabilities of the ESCHER instrument allows eV-TEM to be combined with **E**lectron **E**nergy-**L**oss **S**pectroscopy (EELS) (explained in section 2.1.4). We can therefore determine the energy spectrum of transmitted LEE.

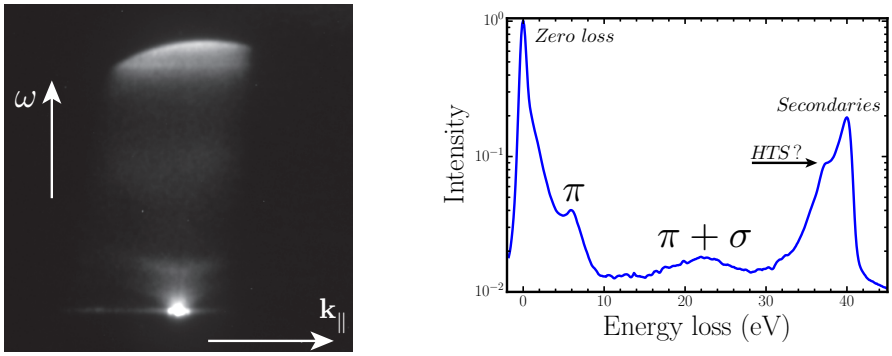

(a) eV-TEM EELS $E_p = 40$ eV

(b) Line scan

Figure 5.2: (a) Energy loss spectrum of transmitted electrons with a primary energy of 35 eV through graphene (mostly double layer; the intensity has a logarithmic scale). **(b)** Line scan of **(a)** around $q = 0$, showing the π-plasmon, $\pi + \sigma$-plasmon and the secondary electrons. In the secondary electron spectrum a feature can be identified 2.3 eV away from the maximum loss. This could be the consequence of a high-transmission state. However, in (a) we do not observe the expected q-dispersion as seen in the ARRES measurements of such high-transmission states (which have a k-dispersion).

Figure 5.2a shows the energy spectrum of electrons that have been transmitted through a graphene double layer. The incident electrons entered the sample with a primary electron energy of 37 eV. The horizontal axis represents the transferred momentum, $\mathbf{k}_{\parallel}$, and the vertical axis the transferred energy, ω. Several features can be identified in this spectrum. First, there is a high intensity around $\mathbf{k}_{\parallel} = 0$ and $\omega = 0$. These electrons transferred very little energy and momentum. These include elastically and quasi-elastically (electron-phonon interaction) scattered electrons.

Above this signal in the spectrum another feature can be seen. This starts at $\omega \approx 5$ eV and shows an approximately linear $\mathbf{k}$-dispersion, resulting in a V-shape in the loss-spectrum. This loss is associated with the excitation of a π-plasmon. The π-plasmon is a collective excitation of the π valence electrons and originates from the $\pi \rightarrow \pi^*$ transition [6]. At higher energy we find a broader feature with a maximum around 20 eV. This is associated with the $\pi + \sigma$-plasmon excitation in which all the valence electrons are involved [6].

At the top of this spectrum, where the transferred energy almost equals the primary electron energy, we find another prominent feature. These are secondary electrons and not primary electrons that lost energy. Such electrons are therefore not part of the loss spectrum. In this secondary electron tail of the EELS spectrum, a feature can be identified 2.3 eV away from the maximum loss (indicated by "HTS?" in figure 5.2b). This could be the consequence of a high-transmission state acting as an intermediate state. However, in figure 5.2a we observe this feature at a constant ω for different $\mathbf{k}$. Thus, we do not see the expected k-dispersion we observed in the ARRES measurements of such high-transmission states.

5.4 Comparing transmission and reflection

In the diffraction-plane, the forward/backscattered electrons can be distinguished from electrons that transferred energy or in-plane momentum to the sample (figure 5.1). We refer to the latter as the scattered electrons. These electrons can be filtered from the image using a contrast aperture, as explained in section 2.1.4. Thus, the reflected and transmitted signals are not always each other's complement because of electron scattering, as seen in chapter 4.

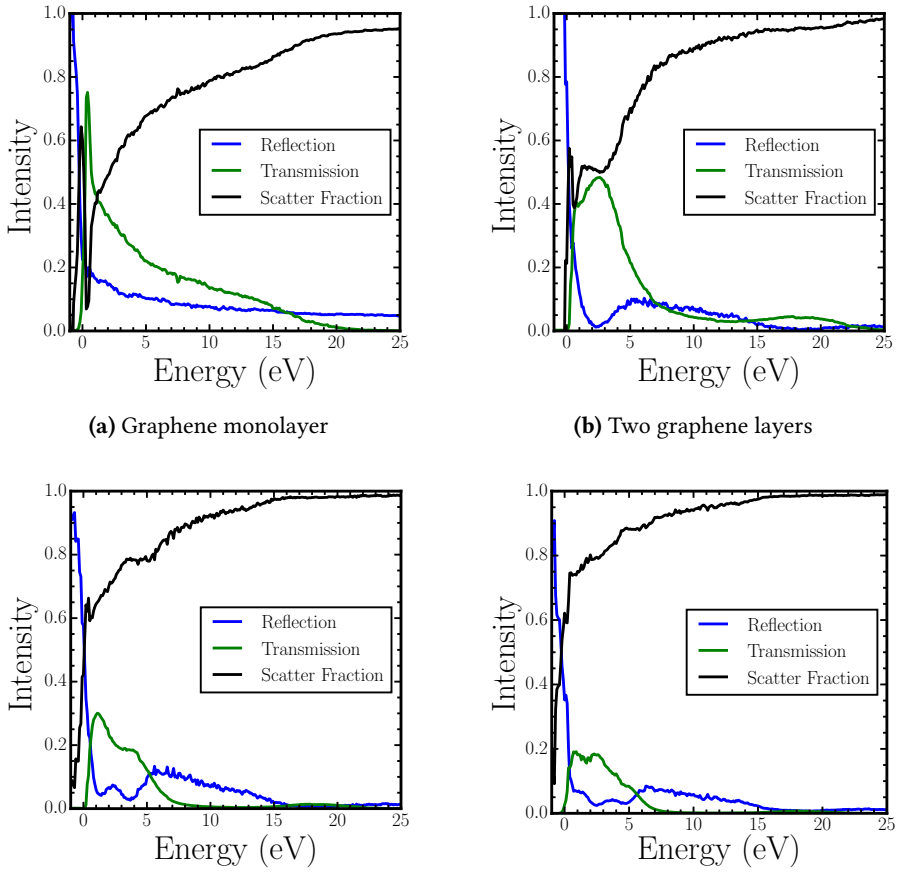

(a) Graphene monolayer

(b) Two graphene layers

(c) Three graphene layers

(d) Four graphene layers

Figure 5.3: LEE reflection (blue), transmission (green) spectra and the scatter fraction (black) of monolayer, bilayer, triple-layer and quadruple-layer graphene respectively in **(a)**-**(d)**. Because of electron scattering reflected and transmitted signals are not each others complement. The scattered fraction, $S(E)$, can be determined by comparing the sum of both signals, $R(E)$ and $T(E)$, to unity; $S(E) = 1 - (T(E) + R(E))$. This scattered fraction can be independently determined for regions of different layer thickness, shown in **(a)**-**(c)**. The fraction of scattered electrons quickly increases with energy.

By comparing the energy-filtered reflected and transmitted signals we can determine the fraction of scattered (and absorbed) electrons, $S(E)$. This fraction is given by:

$$S(E) = 1 - (T(E) + R(E)) \tag{5.1}$$

where $T(E)$ is the normalized (filtered) transmitted and $R(E)$ the normalized (filtered) reflected signal. In figure 5.3 we compare the reflection and transmission spectra that have been presented in figure 4.4 in the previous chapter. This allows us to determine $S(E)$ for multilayer graphene of different thicknesses [*].

In mirror mode, the scatter fraction is zero. When mirror mode is crossed, $S(E)$ increases with energy. This shows that more loss processes become available when the electron energy is increased. However, $S(E)$ is not a direct measure of the available loss processes. When the electron energy corresponds to the energy of a high-transmission state, the probability to excite a loss process is amplified. Note that at constructive interference in transmission, the effective travel length of an electron wave is maximal, the wave 'bouncing' back and forth various time. This is a result of quantum interference. In chapter 1 (figure 1.6c), we show that even with a completely flat absorption spectrum, the scatter fraction has structure.

5.4.1 Mean free paths

In chapter 1 we introduced the electron mean free path universal curve. This suggests that the electron mean free path is long at low electron energies. Now we are in a position to quantify this important length scale for the case of graphene and test if our data are in line with the universal curve.

In the previous chapter we observed that reflection and transmission spectra depend non-trivially on the number of graphene layers. There is however a clear reduction in the transmission signal with layer number (see figure 4.4). In figure 5.4a we plot

$$\lambda_{tot}(E) = \frac{-D}{\ln(T(E))} \tag{5.2}$$

[*] Note that when an incident electron ends up in an unoccupied state between the Fermi and the vacuum level, due to a loss process, the electron will not leave the material (it is absorbed). This is also included in $S(E)$.

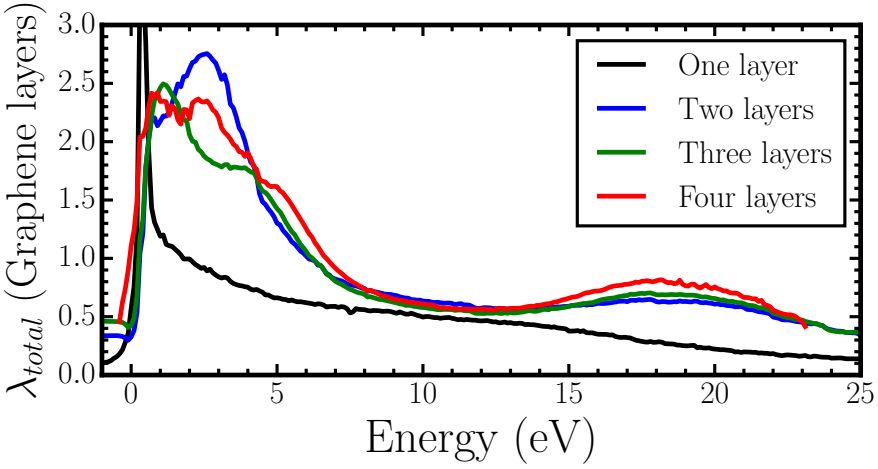

(a) Total mean free path

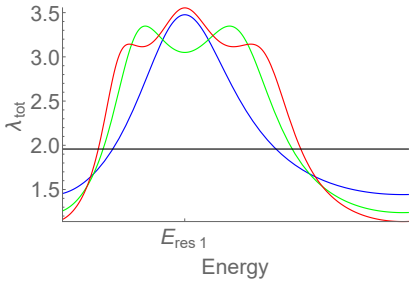

(b) $T = 0.6$, $R = 0.2$

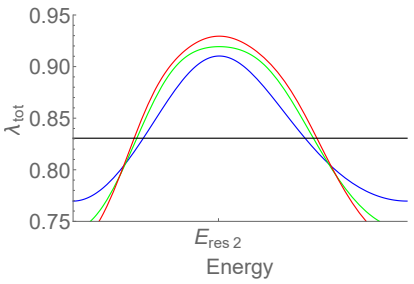

(c) $T = 0.3$, $R = 0.1$

Figure 5.4: (a) Total mean free path, λ_{tot} (equation 5.2), determined in the same way from the transmission spectra presented in figure 4.4b. **(b),(c)** λ_{tot} determined with the results of the transfer matrix calculation method. In (b) we chose $T = 0.6$ and $R = 0.2$, and in (c) we chose $T = 0.3$ and $R = 0.1$. This way, (c) has a higher scatter fraction (i.e. loss) than (b).

where D is the normalized sample thickness (in number of graphene layers) and $T(E)$ the transmissivity of the material as a function of energy. λ_{tot} is the sample thickness (i.e. number of graphene layers, the distance between the layers is 3.4 Å [7]) that transmits a fraction $1/e$ of the incident electrons. With the exception of monolayer graphene and some deviation due to the high-transmission states, λ_{tot} does not strongly depend on layer thickness. For all multilayer thicknesses, the highest measured transmission, in figure 5.4a, is observed in the energy range of the high-transmission states, between 0 and $\sim$ 7eV. The electron mean free path is much smaller than expected from the universal curve.

To compare these data with the results from the model presented in chapter 1, we also determined λ_{tot} from the transfer matrix calculations, following equation 5.2 (see figure 5.4b). Here too, λ_{tot} of the different layer thicknesses oscillates around the same value at the high-transmission states. Moreover, at resonance, λ_{tot} of multilayer graphene is larger than λ_{tot} of the single graphene layer. These results are thus in accordance with the observations in figure 5.4a.

At higher energies, in figure 5.4a, between ~ 7 and ~ 15eV, λ_{tot} is small due to the absence of high-transmission states in that energy range. In the energy regime between ~ 15 and ~ 24 eV, λ_{tot} is larger again for the multilayers. This coincides with the next order high-transmission states. In these higher-order transmission states, λ_{tot} is smaller than in the lower order transmission states. This is a consequence of inelastic processes. Interestingly, in this energy regime with higher loss, λ_{tot} increases with layer number. This can be compared to the λ_{tot} we infer from a transfer matrix model that does incorporate losses. Here we have chosen $T = 0.3$ and $R = 0.1$ (figure 5.4c). Note that the individual interference peaks for multilayer graphene can no longer be distinguished, both in the data (for $15 - 25$ eV) and the model.

The fact that multilayer graphene has a higher λ_{tot} than monolayer graphene at the resonances, shows the importance of interference effects on the transmission properties of the system. This is a consequence of the wave nature of LEE electrons; scattering events in multilayer graphene cannot be considered independently. For some incident electron energies the probability of scattering events will be enhanced. While at other energies events are suppressed by quantum interference effects, as discussed in chapter 1.

The fact that λ_{tot} only depends weakly on the layer number is interesting. In LEEM the number of graphene layers can easily be determined from the resonances in the reflection spectrum. For stacks consisting of many layers this becomes infeasible as the individual resonances can no longer be distinguished. However, in transmission the number of layers can also be determined from the transmissivity of the stack. In figure 5.4a we find that for the optimal transmission between 0 and $\sim$ 7 eV, each $\sim$ 2.5 layer contributes to the reduction of the signal by a factor of e. This means that the ability to determine the multilayer graphene thickness is not limited by the resolvability of the resonances but purely by the signal to noise ratio of the measurement [8, 9]. The number of graphene layers can be be determined from the transmitted signal via:

$$D = -\lambda_{tot} \ln\left(T\left(E\right)\right) \tag{5.3}$$

As discussed, the scattering fraction $S\left(E\right)$ (equation 5.1), determined from both the reflection and transmission spectra, contains information about inelastic scattering. As long as the electron energy is below the energy at which higher-order diffracted beams are formed, the elastically scattered electrons will primarily scatter over small angles (see figure 5.1). Since we directly measure the inelastic signal, we can also define an inelastic mean free path, i.e. the number of layers for which a fraction of $1/e$ of the incident current scatters without losing energy*:

$$\lambda_{in}\left(E\right) = \frac{-D}{\ln\left(T\left(E\right) + R\left(E\right)\right)} = \frac{-D}{\ln\left(1 - S\left(E\right)\right)} \tag{5.4}$$

This is plotted in figure 5.5a. λ_{in} quickly decreases with energy. At low energies, oscillations are observed. Since this is determined from the inelastic signal, some of these features can be associated with the onset of inelastic processes. As before, we compare the measured λ_{in} with the results obtained with the transfer matrix method, presented in figures 5.5b and 5.5c. In the model the loss per layer is constant, nevertheless oscillations appear in the multilayer λ_{in} as a consequence of multiple reflections between the layers, i.e. in these high-transmission states. The structure in the measured λ_{in} in figure 5.5a is therefore not just a consequence of the inelastic processes since λ_{in} is not only determined by the number of available processes and their

*Which is another way of saying that the inelastic mean free path is the expected value of the number of graphene layer an electron passes through before losing energy.

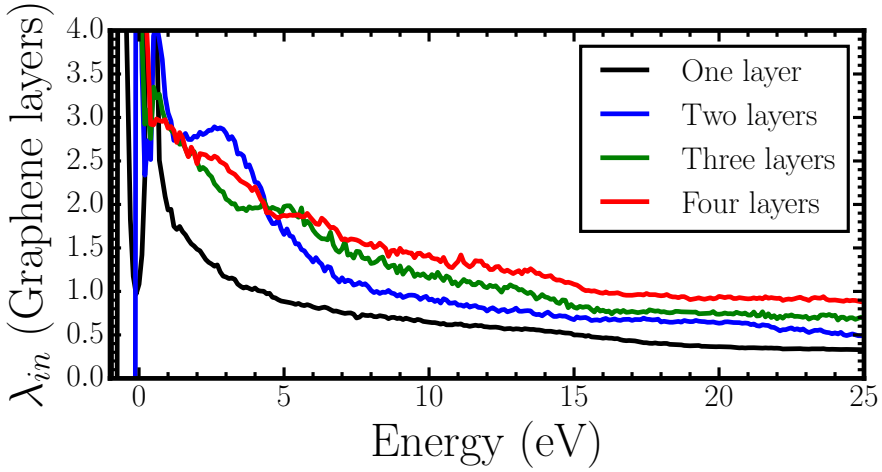

(a) Inelastic mean free path

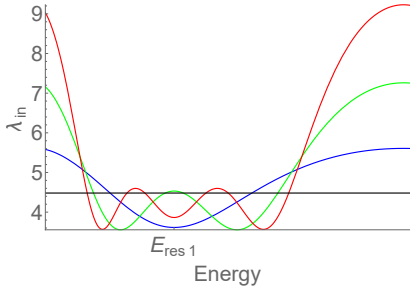

(b) $T = 0.6$, $R = 0.2$

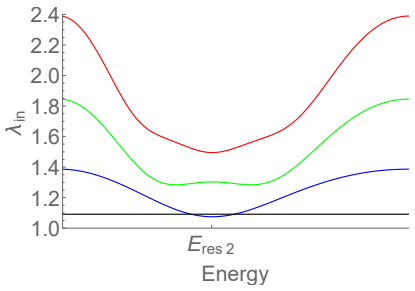

(c) $T = 0.3$, $R = 0.1$

Figure 5.5: (a) Inelastic mean free path, λ_{in} (equation 5.4), determined from the measurements presented in figure 4.4b. The oscillations between $0 - 7$ eV are a result of the resonant elastic scattering in the high-transmission state. This is in agreement with λ_{in} determined, using equation 5.4, from the results from the transfer matrix calculations presented in **(b)** and **(c)**.

individual cross sections but also by interference effects. In figure 5.5c, λ_{in} is determined with the transfer matrices with a higher loss per layer. This shows that λ_{in} increases with layer number, which is again in agreement with our observations in figure 5.5a.

Our findings demonstrate that the universal curve is not as universal as the name suggests. We find that the transmissivity of multilayer graphene is strongly influenced by interference effects as a consequence of inelastic scattering. This does not only influence the reflectivity and transmissivity of the material, it also affects the likelihood an incoming electron excites an inelastic process. Nevertheless, we do find that in general the transmissivity decreases as the energy is increased while for energies above 30 eV, we observe an increase in T again. This is in accordance with the universal curve.

5.5 Discussion and outlook

We have shown that eV-TEM in combination with LEEM can be used to study inelastic scattering with EELS or by comparing the reflection and transmission signals.

The EELS spectra of multilayer graphene clearly show features that are associated with the excitation of the π and $\pi + \sigma$-plasmons [6]. In the EELS measurement secondary electrons can also be identified. Interestingly, there is no clear specific feature in the loss spectrum responsible for the generation of these secondaries. This seems to indicate plural inelastic scattering. A single incident electron can generate multiple secondary electrons. In such processes the current is not conserved. This explains the relatively high intensity in the secondary 'tail' of the loss spectrum.

In figure 5.3 we see that the fraction of inelastically scattered electrons ($S(E)$) increases with energy. This confirms our expectations that as the energy increases, more inelastic scattering processes become available. However, $S(E)$ (which is defined as $1 - T(E) - R(E)$) is not directly related to the number of available loss processes. This becomes immediately clear from the results of the transfer matrix calculations from chapter 1 where we observe oscillations in the scatter fraction, even when the number of available loss processes remains constant.

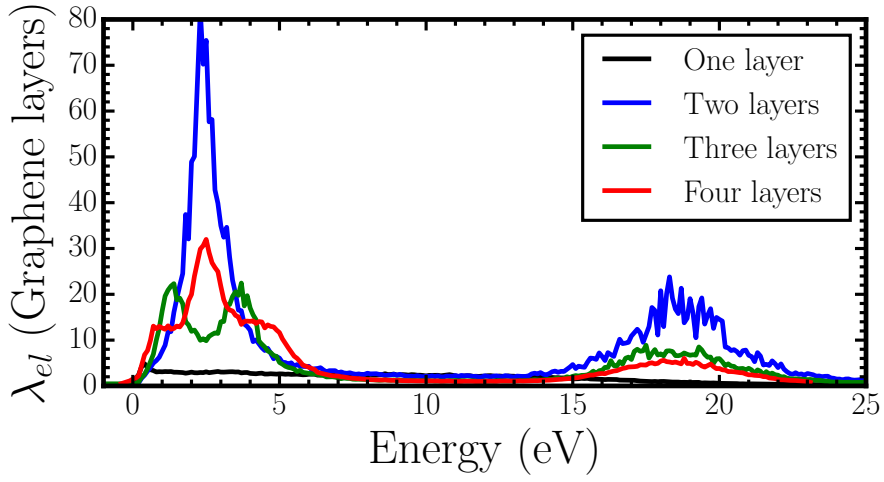

(a) Elastic mean free path

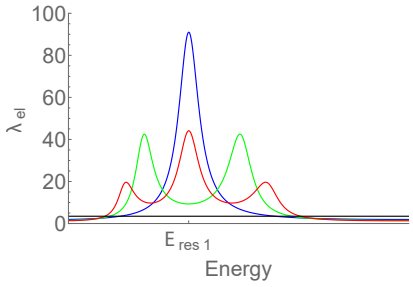

(b) $T = 0.6$, $R = 0.2$

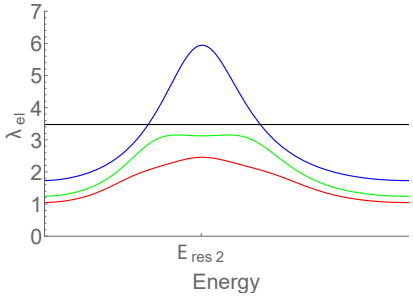

(c) $T = 0.3$, $R = 0.1$

Figure 5.6: (a) Elastic mean free path, λ_{el} (equation 5.6), determined from the measurements presented in figure 4.4b. The high-transmission states are clearly visible here. The states are broadened as a consequence of inelastic processes. **(b)**, **(c)** λ_{el} determined from the results of the transfer matrix calculations.

Since we directly measure λ_{tot} and λ_{in}, we can investigate the elastic mean free path as well. Since an electron can only scatter either elastically or inelastically, we can use Matthiessen's rule:

$$\lambda_{tot}^{-1} = \lambda_{in}^{-1} + \lambda_{el}^{-1} \tag{5.5}$$

to determine λ_{el} from equations 5.2 and 5.4. This gives us:

$$\lambda_{el}(E) = \frac{-D}{\ln(T(E)) - \ln(T(E) + R(E))} = \frac{-D}{\ln\left(\frac{T(E)}{T(E)+R(E)}\right)} \tag{5.6}$$

which is plotted in figure 5.6. The high-transmission states can clearly be identified. At higher energies, the states are broadened as a result of inelastic effects. This shows that the elastic and inelastic processes influence each other and cannot simply be studied separately.

The loss spectra are not only affected by inelastic scattering but also by interference effects due to elastic scattering. The likelihood of exciting an inelastic process is therefore a property of the sample as a whole. To study the likelihood of loss processes in its constituents, interference effects have to be taken into account. In chapter 1 we presented a method to predict the interference effects. However, this one-dimensional model does not accurately predict the precise energies of the resonances. Calculations that take the three-dimensional nature of the multilayer graphene potential into account should be performed [10, 11]. Since the electronic structure differs between mono- and multilayer graphene, we expect to find different loss processes.

The reason that the wavelike properties of the electron play such an important role in the interpretation of our results is because sample thickness is smaller than the electron coherence length and the electron λ_{tot} (i.e. $d < \lambda_{tot} \approx x_l$, where d is the sample thickness and x_l the electron coherence length). Since graphene is a highly-ordered material, it is possible to construct an accurate theoretical model to interpret the results with conventional techniques. The case for which $x_l > d > \lambda$ is much more complex. This situation describes a thin inhomogeneous sample. Interference effects in the sample lead to an electron speckle pattern. Such a pattern will be very difficult to interpret. Nevertheless, such a pattern contains a lot of the information of the interactions electrons undergo in the material and is therefore very interesting. Finally there is the situation in which $x_l \approx \lambda_{tot} \ll d$ where interference effects can be neglected. In this classical limit, consecutive scattering events can

be considered independent [12]. This makes the interpretation of the results much easier. Unfortunately, since decoherence is by definition associated with information loss, it is impossible to reconstruct all the interactions the electron underwent in the material.

The combination of eV-TEM and LEEM allows us to study the mechanisms involved in radiation damage. This is of special interest to study radiation damage in biological materials, but also other organic compounds. In chapter 6 we study the effects of radiation damage on PMMA by LEEM .

References

1. Egerton R. F. Electron energy-loss spectroscopy in the TEM. *Reports on Progress in Physics* **72,** 016502 (2009).
2. Egerton R. F., Wang F. & Crozier P. A. Beam-Induced Damage to Thin Specimens in an Intense Electron Probe. *Microscopy and Microanalysis* **12,** 65–71 (2006).
3. Politano A., Marino A. R., Campi D., Farías D., Miranda R. & Chiarello G. Elastic properties of a macroscopic graphene sample from phonon dispersion measurements. *Carbon* **50,** 4903–4910 (2012).
4. Egerton R. *Electron Energy-Loss Spectroscopy in the Electron Microscope* ISBN: 978-1-4419-9582-7 (Springer US, Boston, MA, 2011).
5. Locatelli A., Knox K. R., Cvetko D., Menteş T. O., Niño M. A., Wang S., Yilmaz M. B., Kim P., Osgood R. M. & Morgante A. Corrugation in Exfoliated Graphene: An Electron Microscopy and Diffraction Study. *ACS Nano* **4,** 4879–4889 (2010).
6. Politano A. & Chiarello G. Plasmon modes in graphene: status and prospect. *Nanoscale* **6,** 10927–10940 (2014).
7. Ohta T. Controlling the Electronic Structure of Bilayer Graphene. *Science* **313,** 951–954 (2006).
8. Frank L., Mikmeková E., Müllerová I. & Lejeune M. Counting graphene layers with very slow electrons. *Applied Physics Letters* **106,** 013117 (2015).
9. Mikmeková E., Frank L., Müllerová I., Li B. W., Ruoff R. S. & Lejeune M. Study of multi-layered graphene by ultra-low energy SEM/STEM. *Diamond and Related Materials* **63,** 136–142 (2016).
10. Feenstra R. & Widom M. Low-energy electron reflectivity from graphene: First-principles computations and approximate models. *Ultramicroscopy* **130,** 101–108 (2013).
11. Krasovskii E. E. in *Solid-State Photoemission and Related Methods* 220–246 (Wiley-VCH Verlag GmbH, Weinheim, Germany, 2003). ISBN: 3527403345.
12. Naaman R. & Sanche L. Low-Energy Electron Transmission through Thin-Film Molecular and Biomolecular Solids. *Chemical Reviews* **107,** 1553–1579 (2007).